UDC 624.012.45

# STUDIES OF THE STRESS-STRAIN STATE OF THE SUPPORT ZONES
# OF REINFORCED CONCRETE BEAMS WITH CLIPPED BY THE FINITE ELEMENT METHOD

*AMJAD SULAIMAN ALNAHDI*
**Polotsk State University, Belarus**

*KHALED ABDO AL HALEM ALROBASSI*
**Aden State University, Yemen**

*This paper deals with the nonlinear finite element analysis of two shear-critical concrete dapped-end beams. Reinforced concrete dapped-end beams having nominal shear span to depth ratio values of 0.56 and 0.59, concrete strength 32 MPa and 34 MPa, and reinforcement ratio via yield strength 2.83 MPa and 7.39 MPa, that failed in shear have been analyzed using the 'ANSYS' program. The 'ANSYS' model accounts for the nonlinearity, such as, post cracking tensile stiffness of the concrete, stress transfer across the cracked blocks of concrete. The concrete is modeled using 'SOLID65'– eight-node brick element, which is capable of simulating the cracking and crushing behavior of brittle materials. The internal reinforcements have been modeled discretely using 'LINK8' – 3D spar element. A parametric study is also made to explain the effects of variation of some main parameters such as shear span to depth ratio, concrete compressive strength, and the parameter of main dapped-end reinforcement on the behavior of the beams. From the present modality the capability of the model to capture the critical crack regions, loads and deflections for various types of shear failures in reinforced concrete dapped-end beams have been illustrated. The parametric study shows that the beams shear strength is affected by the shear span to depth ratio, concrete compressive strength and the amount of main reinforcement.*

Notations

$a$  – *S*hear span measured from the center of support to the center of hanger bars $(\text{mm})$

$d$  – Effective depth of the nib $(\text{mm})$

$As$ – Area of the main dapped-end Reinforcement $(\text{mm}^2)$

$f_c{}'$ – Compressive strength of the concrete cylinder $(\text{MPa})$

$f_t$ – Tensile strength of concrete $(\text{MPa})$

$f_y$ – Yield stress of the steel reinforcing bars. $(\text{MPa})$

$P_u$ – Failure load $(\text{kN})$

$V_d$  – Shear strength of dapped-end beam $(\text{kN})$

$V_{d,\,test}$ – Shear strength of the dapped-end beam measured in the test $(\text{kN})$

ρ  – Ratio of the main dapped reinforcement

**Introduction.** The dapped-end concrete beams enable the construction depth of a precast concrete floor or roof structure to be reduced, by recessing the supporting corbels into the depth of the beams supported [1]. They are mainly used in drop-in beams between corbels Fig. 1, *a*, as part of beam-to-beam connection Fig. 1, *b* and in suspended spans between cantilevers Fig. 1, *c*. The use of dapped-end beams facilitates the erection of a precast concrete structure, due to the greater lateral stability of an isolated dapped-end beam than that of an isolated beam supported at its bottom face [2].

A series of studies on dapped-end beams have investigated the influence of effective span to depth ratio and different main, anchorage, and web reinforcements on the behavior of reinforced concrete dapped-end beams [1– 4, 7–9].

Mattock and Chan, (1979) [1], tested eight dapped-end beams. Four beams being subjected to vertical load only and four to a combination of vertical and horizontal loads.
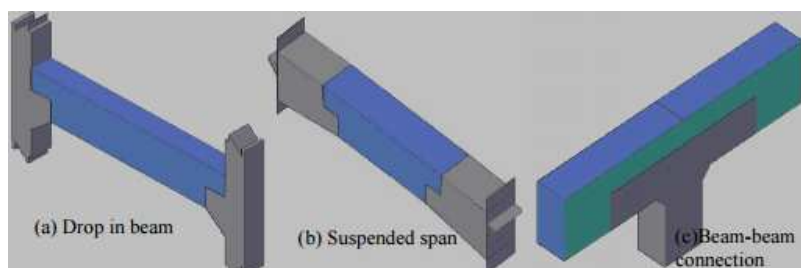


Fig. 1. Application of dapped-end beams

The dimensions of beams and amount of reinforcement in each specimen are listed in Table 1. From the test results the authors' inclusions were the followings:

1. The reduced depth part of the dapped end may be designed as if it were a corbel, using the design proposal of Mattock, providing the shear span (*a*) used in design is taken equal to the distance from the center of action of vertical load to the center of the gravity of the hanger reinforcement.

2. The full depth part of the beam should be designed so as to satisfy moment and force component across inclined cracks, in addition to carrying out that the usual design of sections normal to the longitudinal axis of the beam for flexure, shear, and axial force.

3. As shown in Fig. 2.

4. The main nib reinforcement should be provided with a positive anchorage as close to the end face of the beam as possible.

5. A group of closed stirrups having yield strength not less than the nominal shear strength should be provided close to the end face of the full depth beam to resist the vertical component of the inclined compression force in the nib.

6. The horizontal (hoop) stirrups should be positively anchored near the face of the beam by wrapping around vertical bars in each corner. As shown in Fig. 2.

Table 1. – Specimen reinforcement details and concrete strength [1]

| spec. no. | Main dapped-end reinforcement | | | Hoops horizontal reinforcement | | | Hanger reinforcement | | | Concrete strength | a/d | $\rho f_y$ |
|---|---|---|---|---|---|---|---|---|---|---|---|---|
| | Bars | $A_s(mm^2)$ | $f_y$ (MPa) | Stir. | $A_h(mm^2)$ | $f_y$(MPa) | Stir. | $A_{sh}(mm^2)$ | $f_y$ (MPa) | $f'_c$ (MPa) | mm/mm | MPa |
| 1A | 2#3 | 141.9 | 476.4 | 1#2 | 64.5 | 461.9 | 3#3 | 425.8 | 451.6 | 33.6 | 0.59 | 1.89 |
| 1B | 2#6 | 567.7 | 412.3 | 2#2 | 129.0 | 455.0 | 3#3 | 425.8 | 466.7 | 30.5 | 0.59 | 6.54 |
| 2A | 3#3 | 212.9 | 478.5 | 2#2 | 129.0 | 461.9 | 2#3 | 283.8 | 462.6 | 32.9 | 0.59 | 2.85 |
| 2B | 2#6 | 567.7 | 412.3 | 2#2 | 129.0 | 460.5 | 2#3 | 283.8 | 470.2 | 30.8 | 0.59 | 6.54 |
| 3A | 3#3 | 212.9 | 476.4 | 2#2 | 129.0 | 448.1 | 2#3 +1#2 | 283.8 +64.5 | 470.2 448.1 | 37.0 | 0.59 | 2.83 |
| 3B | 2#6 | 567.7 | 438.5 | 2#2 | 129.0 | 484.0 | 2#3 +1#2 | 283.8 +64.5 | 488.8 484.0 | 31.6 | 0.59 | 6.95 |
| 4A | 3#3 | 212.9 | 476.4 | 2#2 | 129.0 | 435.7 | 2#3 +1#2 | 283.8 +64.5 | 488.8 484.0 | 31.6 | 0.59 | 2.83 |
| 4B | 2#6 | 567.7 | 438.5 | 2#2 | 129.0 | 461.9 | 2#3 +1#2 | 283.8 +64.5 | 488.8 484.0 | 31.6 | 0.59 | 6.95 |

*Stir.* = *Stirrups* $\rho$

$f_y = As / bd * f$
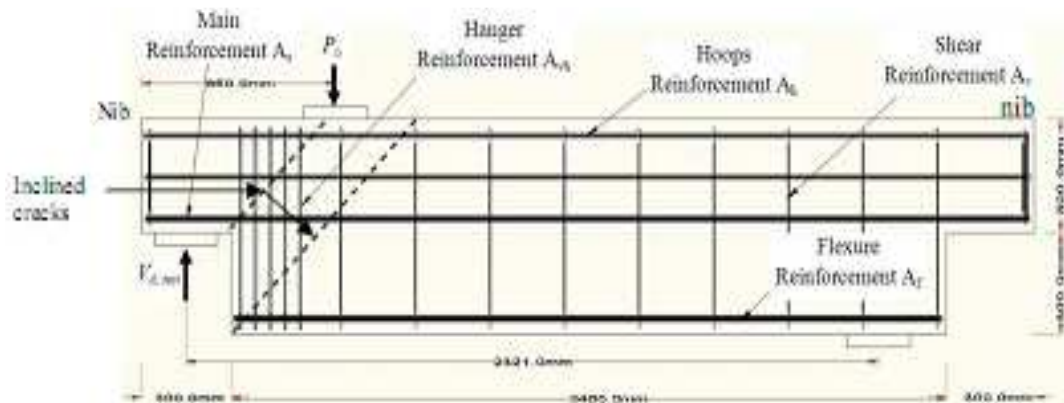


Fig. 2. Dimensions and reinforcement details of beam B56, *a/d* = 0.56 [2]

Twelve high-strength concrete dapped-end beams were tested by Wen-Yao Lu, et al, (2003) [2], as listed in Table 2, to study the shear strength of dapped-end beams of the concrete strength, the amount of main dapped-end reinforcement, and the nominal shear span-to-depth ratio. The details of the tested specimens are listed in Table 2. The test results indicate that the shear strength of dapped-end beams increases with the increase of the concrete strength, the amount of main dapped- end reinforcement, and the decrease of nominal shear span-to-depth ratio.

Table 2. – Specimen reinforcement details and concrete strength [2]

| spec. no. | Main dapped-end reinforcement | | | Hoops horizontal reinforcement | | | Hanger reinforcement | | | Concrete strength | a/d | $\rho f_y$ |
|---|---|---|---|---|---|---|---|---|---|---|---|---|
| | Bars | $A_s(mm^2)$ | $f_y$ (MPa) | Stir. | $A_h(mm^2)$ | $f_y$(MPa) | Stir. | $A_{vh}(mm^2)$ | $f_y$ (MPa) | $f'_c$ (MPa) | mm/mm | MPa |
| 1 | 3#6 | 859.6 | 461.8 | 2#3 | 285.3 | 368 | 5#4 | 1266.8 | 430.14 | 34.0 | 0.56 | 7.39 |
| 2 | 3#6 | 859.6 | 461.8 | 2#3 | 285.3 | 368 | 6#4 | 1520.2 | 430.14 | 62.6 | 0.59 | 7.39 |
| 3 | 3#6 | 859.6 | 461.8 | 2#3 | 285.3 | 368 | 6#4 | 1520.2 | 430.14 | 69.2 | 0.59 | 7.39 |
| 4 | 3#6 | 859.6 | 461.8 | 2#3 | 285.3 | 368 | 6#3 | 856.0 | 416.14 | 34.0 | 0.89 | 7.39 |
| 5 | 3#6 | 859.6 | 461.8 | 2#3 | 285.3 | 368 | 4#4 | 1013.4 | 430.14 | 62.6 | 0.83 | 7.39 |
| 6 | 3#6 | 859.6 | 461.8 | 2#3 | 285.3 | 368 | 4#4 | 1013.4 | 430.14 | 69.2 | 0.81 | 7.39 |
| 7 | 2#6 | 573.0 | 461.8 | 2#3 | 285.3 | 368 | 4#4 | 1013.4 | 430.14 | 33.7 | 0.52 | 5.08 |
| 8 | 2#6 | 573.0 | 461.8 | 2#3 | 285.3 | 368 | 4#4 | 1013.4 | 430.14 | 62.6 | 0.54 | 5.08 |
| 9 | 2#6 | 573.0 | 461.8 | 2#3 | 285.3 | 368 | 4#4 | 1013.4 | 430.14 | 69.2 | 0.54 | 5.08 |
| 10 | 2#6 | 573.0 | 461.8 | 2#3 | 285.3 | 368 | 5#3 | 713.3 | 416.14 | 33.7 | 0.83 | 5.08 |
| 11 | 2#6 | 573.0 | 461.8 | 2#3 | 285.3 | 368 | 5#3 | 713.3 | 416.14 | 62.6 | 0.84 | 5.08 |
| 12 | 2#6 | 573.0 | 461.8 | 2#3 | 285.3 | 368 | 5#3 | 713.3 | 416.14 | 69.2 | 0.85 | 5.08 |

$Stir. = Stirrups \rho$

$f_y = As / bd * f$

The comparison between test results and an analytical proposed model given by Lu, et al. [2] shows that it can predict the shear strength of reinforced concrete dapped-end beams more accurately than the approach of the PCI-Design Handbook [2].

Ronnie R.H. and et al, (2003) [3], are proposed compatibility-aided trut-and-tie model (CASTM), for predicting the diagonal crack widths at re-entrant corners of dapped ends of bridge girders and the ledges of inverted T bent caps. The validity of this model is supported by tests of seven full-scale specimens. From comparison CASTM with tests large diagonal cracks occur at the re-entrant corners of dapped ends of bridge girders and the ledges of inverted T bent caps. These diagonal crack widths can be predicted by the proposed CASTM, and the proposed CASTM is calibrated by large test specimens simulating bridge structures. They proposed that the calibrated gage length should be applicable to all concrete bridges.

**1. Research Objective.** The objective of this paper is to study the ultimate shear behavior of a reinforced concrete dapped-end beams using three-dimensional finite element analysis approach on the reinforced concrete dapped-end beams ultimate shear behavior. For this purpose, two reinforced concrete dapped-end beams with span to depth ratio (0.56, 0.59) were analysis in finite element solutions were obtained by using ANSYS program [10]. The experimental and finite element modeling results are compared numerically and graphically.

**2. Description of Analyzed Beams.** Two experimental reinforced dapped-end beams were analyzed in this study. The first beam has shear span to depth ratio a/d equal to 0.56, and the second beam with shear span to depth ratio a/d equal to 0.59, as illustrated below:

**2.1. Details of Dapped-End Beam B56.** The first was tested by Lu et al. [2] dapped-end beam had constant span and width of 3000mm and 200mm, respectively. The overall depth was 600mm, and the shear span to depth ratio was 0.56 (i.e. a = 150 mm, d = 268 mm). The beam sample B56 refer to beam with (a/d = 0.56). The reinforcement of beam and properties are summarized in Table 2 and Fig. 2. The beam notation (1) denotes the beams from reference (2). The typical beam details and geometry is shown in Fig. 2 [2].

**2.2. Details of Dapped-End Beam B59.** The second beam was tested by Mattock and Chan [1] has constant span and width of 3000 mm and 127 mm, respectively. The overall depth was 610 mm, and the shear span to depth ratio of the beam is 0.59 (i.e. a = 165 mm, d = 280 mm), The beam sample B59 refer to beam with (a/d = 0.59). The reinforcement of beam and properties are summarized in Table 2 and Fig. 3. The beam notation (4A) denotes the beams from reference (1). The typical beam details and geometry is shown is shown in Fig. 3 [1].
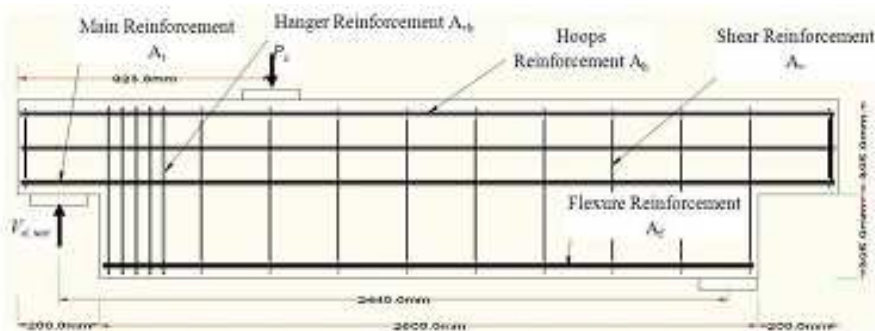


Fig. 3. Dimensions and reinforcement details of beam  B59, a/d = 0.59 [1]

**3. Finite Element Analysis and Nonlinear Solution Technique.** Finite element analysis has been performed in the present work using the ANSYS program [10] which is capable of handling dedicated numerical models for the nonlinear response of concrete under static and dynamic loading.

**3.1. Element Types.** The element type of concrete is eight-node solid brick element (SOLID 65) used for modelling the concrete. This element type includes a smeared crack analogy for cracking in tension zones and a plasticity algorithm to account for the possibility of concrete crushing in compression regions. it has eight corner nodes with three degrees of freedom for each: translations in x, y, and z directions. The eight-node solid element, SOLID 45, has been used for the steel plates, to represent the load plates and the beam supports. The element is also defined by eight nodes with three translational degrees of freedom for each node in x, y, and z directions, with plasticity, creep, swelling, stress stiffening, large deflection, and large strain capabilities. A reduced integration option with hourglass control is available. For Steel reinforcement the 3D spar element (LINK 8) which allows the elastic – perfectly plastic response of the reinforcing bars has been used. Two nodes are required for this element. Each node has three degrees of freedom: translations in the nodal x, y, and z directions.

Three material models have been adopted in the present study the; Material Model Number 1 refers to the SOLID 65 element for concrete. The SOLID 65 element requires linear isotropic and multi-linear isotropic material properties to properly model concrete. The multi-linear isotropic material uses the von Mises failure criterion along with the William and Warnke [12] model to define the failure of the concrete. EX is the modulus of elasticity of the concrete (Ec), and PRXY is the Poisson's ratio (υ). The modulus of elasticity was based on Equation (1) [5]

$$E_c = 4730\sqrt{f_c^{/}} \qquad \left(f_c^{/} \mathrm{MPa}\right). \tag{1}$$

A nonlinear elasticity model was adopted for concrete. The compressive uniaxial stress-strain relationship for the concrete model was obtained using the following equations to compute the multi-linear isotropic stress-strain curve for the concrete (MacGregor 1992) [14].

$$f = \frac{E_c.\varepsilon}{1-\left(\dfrac{\varepsilon}{\varepsilon_0}\right)^2} \quad , \varepsilon_0 = \frac{2f_c^{/}}{E_c}, \;\; E_c = \frac{f}{\varepsilon} \tag{2}$$

where $f$ = stress at any strain $\varepsilon$, MPa;

$\varepsilon$ = strain at stress $f$;

$\varepsilon_0$ = strain at stress $f_c$'.

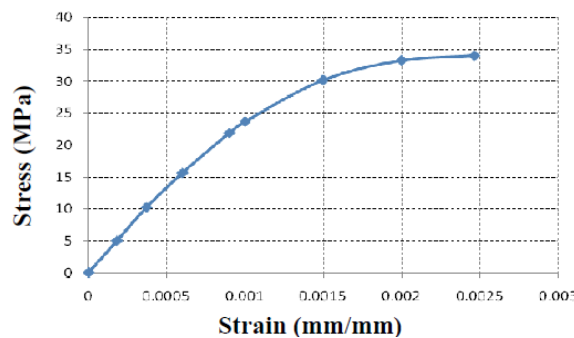For our concrete, the obtained stress–strain model is shown in Fig. 4.



Fig. 4. Uni-axial stress-strain curve for concrete

The Poisson ratio is taken as 0.2. The ultimate uni-axial compressive strength of concrete is taken from the mean value of cylinder concrete compressive strength. The tensile strength of concrete is assumed to be equal to the value given below [12].

$$f_t = 0.62\sqrt{f_c^{/}} \qquad \left(f_c^{/} \mathrm{MPa}\right). \tag{3}$$

The implemented multi-linear isotropic stress–strain relationship requires the first point of the curve to be defined by the user. It must satisfy Hooke's Law.

The shear transfer coefficient for open cracks, $\beta_t$, represents the conditions at the crack face. The value of $\beta t$ ranges from 0.0 to 1.0, with 0.0 representing a smooth crack (complete loss of shear transfer) and 1.0 representing a rough crack (no loss of shear transfer). Shear transfer coefficient of 0.3 is used to derive the theoretical load–displacement relationship for comparison with experimental results [12, 13].

During transition from elastic to plastic or elastic to brittle behavior, two numerical strategies were recommended [16]: proportional penetration, which subdivides proportional loading into an elastic and inelastic portion which governs the failure surface using integration, and normal penetration, which allows the elastic path to reach the yield surface at the intersection with the normal therefore solving a linear system of equations. Both these methods are feasible and give stress values that satisfy the constitutive constraint condition [16].

**3.2. Material Properties.** Steel reinforcement in the experimental beam was constructed with typical steel reinforcing bars as motion in Table 3. Elastic modulus and yield stress for the steel reinforcement used in tests were considered in the finite element modeling of reinforcement. A 50 mm thick steel plate modeled using SOLID45 elements, is added at the support location, and load applied position in order to avoid stress concentration problems. This provides a more even stress distribution over the support area and position of load. An elastic modulus equal to 200 GPa and Poisson's ratio equal to 0.3 are used to plate.

The steel for the finite element models is assumed to be an elastic–perfectly plastic material and identical in tension and compression. Poisson's ratio value of 0.3 is used for the steel reinforcement. Material properties for the concrete and steel reinforcement are summarized in Table 3.

Table 3. – Material properties of the tested beam [1. 2]

| Beam No. | $E_c$ MPa | $A_s$ $mm^2$ | $f'_c$ MPa | $f_t$ MPa | $f_y$ MPa | $E_s$ MPa |
|---|---|---|---|---|---|---|
| B56 | 27,580 | 212.9 | 34.0 | 3.6 | 461.8 | 200,000 |
| B59 | 26,757 | 859.6 | 31.6 | 3.4 | 476.4 | 200,000 |

**3.3. Modeling by ANSYS Code.** The dimension of the full-size beam B56 is 200*600*3000 mm. The span between the two supports was 2321 mm. As shown in Fig. 2 by taking the advantage of the symmetry of the beam, a half of the full beam was used for finite element modeling. The half of the entire model is shown in Fig. 5.

To obtain satisfactory results from the SOLID65 element, a square or rectangular mesh is recommended. Therefore, the mesh was setup such that square elements were created as shown in Fig. 6. Each concrete mesh element is a prism dimensions of $25 \times 25 \times 25$ mm for specimen B56 [14]. The necessary element divisions are noted. The meshing of the reinforcement is a special case compared to the volumes to be omitted as it is a repetition.
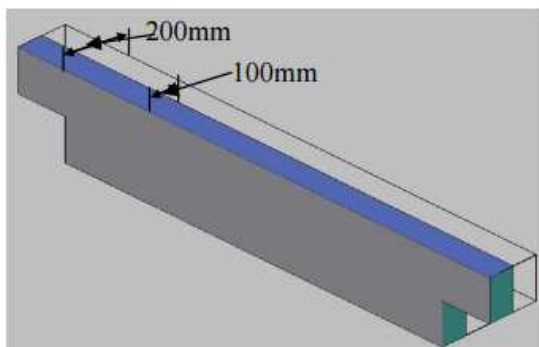


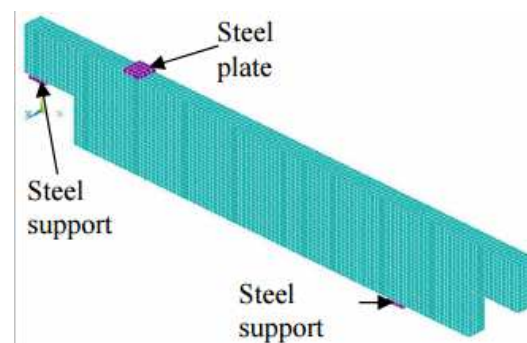Fig. 5. The half of beam model B56



Fig. 6. Finite element mesh of the half beam B56

In nonlinear analysis, the total load applied to a finite element model is divided into a series of load increments called load steps [13]. At the completion of each incremental solution, the stiffness matrix of the model is adjusted to reflect nonlinear changes in structural stiffness before proceeding to the next load increment. The Newton–Raphson equilibrium iterations for updating the model stiffness were used in the nonlinear solutions. Prior to each solution, the Newton–Raphson approach assesses the out-of-balance load vector, which is the difference between there storing forces (the loads corresponding to the element stresses) and the applied loads [15] subsequently.

The program carries out a linear solution using the out-of-balance loads and checks for convergence. If convergence criteria are not satisfied, the out-of-balance load vector is re-evaluated, the stiffness matrix is updated, and a new solution is carried out. This iterative procedure continues until the results converge.

In this study, convergence criteria for the reinforced concrete SOLID elements were based on force and displacement, and the convergence tolerance limits were initially selected by analysis program. It was found that the convergence of solutions for the models was difficult to achieve due to the nonlinear behavior of reinforced concrete. Therefore, the convergence tolerance limits were increased to a maximum of five times the default tolerance limits 0.5% for force checking and 5% for displacement checking) in order to obtain the convergence of the solutions [11, 13].

**4. Comparison of experimental and analytical data.**

**4.1. Load-Deflection Relationship.** The load–deflection responses for the two reinforced concrete dapped-end beam B56, and B59 computed by the present finite element model are plotted in Fig. 7 based the corresponding relationships drawn from the previous experimental investigations [2], and [1], respectively.
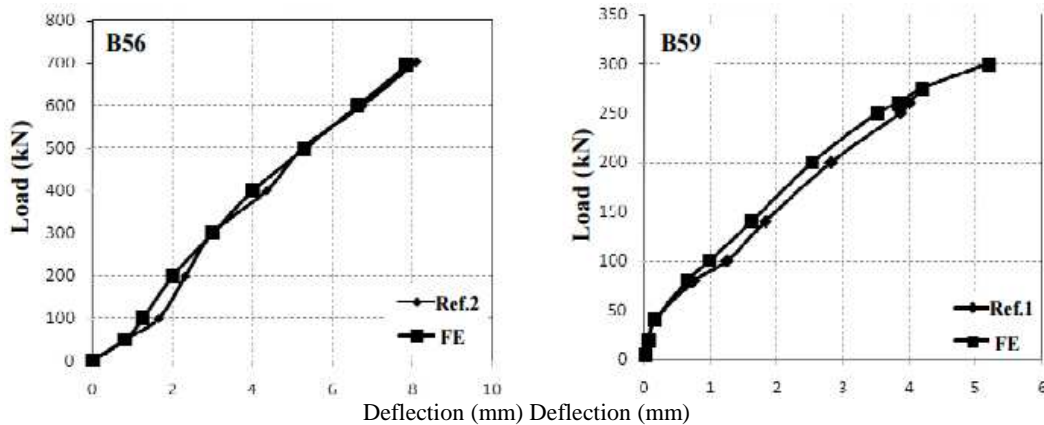


Deflection (mm) Deflection (mm)

Fig. 7. Experimental [1, 2] and FEM loadñdeflection responses

For the dapped-end beam B56 the ultimate loads from the finite element and experimental models are 694 kN and 703 kN, respectively, and the ultimate deflection are 7.8 mm, and 8.1 mm, respectively. For dapped-end beam B59 the ultimate loads from the finite element and experimental models are calculated as 300 kN and 275 kN, respectively, and the ultimate deflection are 4.2 mm, and 5.21 mm, respectively. With reference to Table (4) and Fig. 7 deflections at beam soffits under bad positions given by the previous experimental tests of Ref. [2] and [1], and those computed by the present finite element model are very close to each other.

Table 4. – Comparison of test result [1, and 2], and FE solution

| Beam Notation | Experimental Load (EXP) (kN) | FE Load (kN) | FE / EXP | EXP Ultimate Deflection (mm) | FE Ultimate Deflection (mm) |
|---|---|---|---|---|---|
| B56 | 703 | 694 | 0.98 | 8.1 | 7.8 |
| B59 | 275 | 300 | 1.09 | 4.2 | 5.21 |

The ratio between the experimental and theoretical deflections at ultimate load are 0.99 and 1.09, for beams B56, and B59 are 1.09, respectively. On the other hand, the degree of correlation $R^2$ is 0.99 for both the measured deflection and the applied load for both beams.

In general, the load–deflection plots for the beam from the present finite element analysis agree quite well with the previous experimental data of Ref. [1, and 2]. The finite element load–deflection curve is slightly different from the experimental curve. There are several effects that may cause this situation. First of all, microcracks are present in the concrete for the tested beam and could be produced by drying shrinkage in the concrete and/or handling of the beam. On the other hand, the finite element models do not include the microcracks. The other is that perfect bond between the concrete and steel reinforcing bars is assumed in the finite element analysis, this assumption would not be true for the tested beam. In ANSYS model, stresses and strains are calculated at the integration points of the concrete SOLID elements.

**4.2. Stress Distribution.** The behavior of beams B56 and B59 is considered satisfactory, both at service and ultimate loads. For all specimens the general process of cracking is similar. The first crack initiates at the re-entrant corner at about 12.4%, and 8.45% of ultimate load for beams B56 and B59, respectively. This crack propagated at approximately 45° to the horizontal. It extends to about 2/3 the height of the nib. At this time additional diagonal tension cracks take place in the nib and in the full depth of the beam. Maximum stresses for the last converging load step are shown for the beams in Fig. 8 and 9 where the maximum stress locations in the reinforced concrete dapped-end beams as determined by the present finite element model are shown.
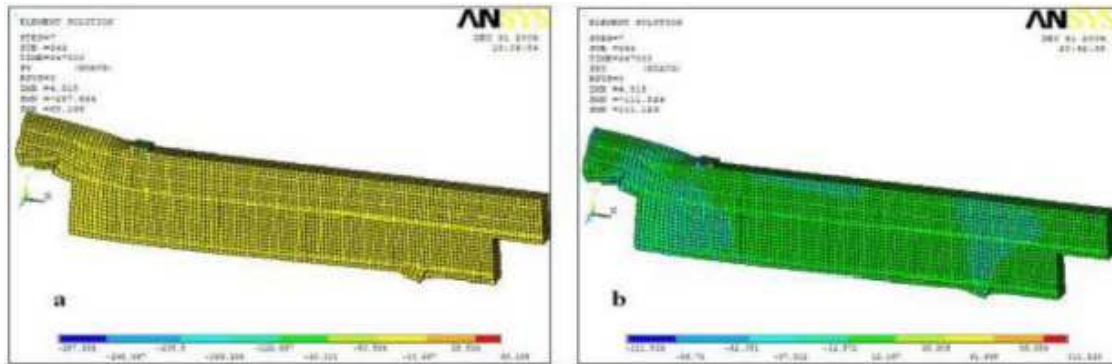
Fig. 8. Maximum stress distribution for beam B56 (MPa), given by the present finite element
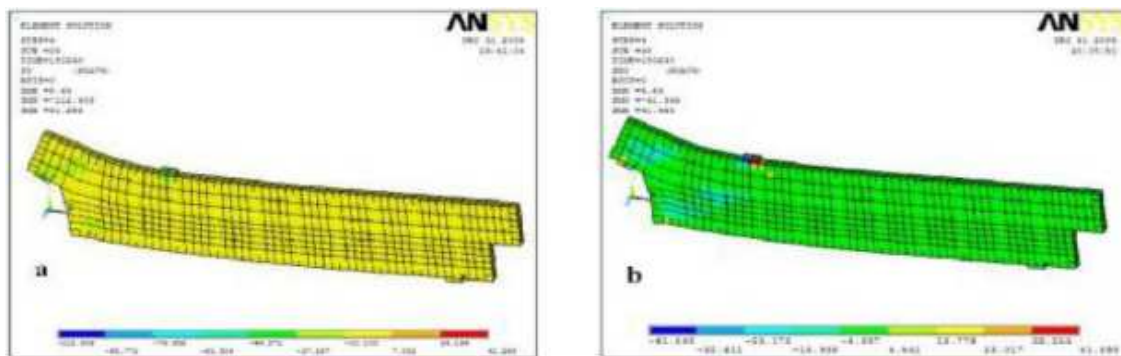model: *a* – Maximum compressive and tensile stresses, *b* – Maximum shear stress



Fig. 9. Maximum stress distribution for beam B59 (MPa), given by the present finite
element model: *a* – Maximum compressive and tensile stresses, *b* – Maximum shear stress

**4.3. Crack Patterns.** The crack patterns obtained from the present finite element analysis at the last converged load steps are shown in Fig. 10, *a* and *b*, from which it can be observed that that numerous cracks occur at midspan of the finite element model at four load levels, the cracks begin at the re-entrant corner of the dapped end beams at load values 56, and 35.5 kN for specimens B56 and B59, respectively.

As the load is further increased additional cracks form and existing cracks lengthen. The diagonal tension crack in the nib assumes a flatter trajectory on reaching the hanger reinforcement, propagating toward the loading plate. This is in agreement with the simulation of strut and ties modeling for deep beam, and corbel with struts (concrete) and ties (the tension steel bars with almost constant stress).

In all cases the main reinforcement yields before maximum load is reached. At that time, the cracks crossing this reinforcement widen noticeably. Shortly before failure, compression spalling and crushing the top face of the beam occurred adjacent to the loading plate. A side face of the half beam model is used to demonstrate cracking sign. As shown in Fig. 10, at the nib of the beam at bottom, cracking signs refer to development normal tensile stresses in the *x* (longitudinal) direction, and shear stresses in the *xz* plane. Consequently, the direction of tensile principal stresses becomes inclined from the horizontal.

Once the principal tensile stresses exceed the ultimate tensile strength of the concrete, tensile cracks perpendicular to the directions of the principal stresses appear at integration points of the concrete finite elements. These are referred as diagonal tensile cracks.

Principal tensile stresses occur mostly in the longitudinal direction. When the principal stresses exceed the ultimate tensile strength of the concrete, cracking signs appear perpendicular to the principal stresses in that direction. Therefore, the cracking signs shown in Fig. 10 appear as vertical straight lines occurring at the integration points of the concrete solid elements. These are referred as flexural cracks. For a concrete structure subjected to uni-axial compression, cracks propagate primarily parallel to the direction of the applied compressive load since the cracks resulting from the tensile strains developed due to Poisson's ratio effect [12, 16]. Similar behavior is seen in Fig. 10 based on the finite element analysis. Loads in the *z* direction result in tensile strains in the *y* direction by Poisson's effect. Thus, circles appear perpendicular to the principal tensile strains in the y direction at the integration points in the concrete elements near the loading location referring to as compressive fracture.

In all cases the main reinforcement yields before maximum load is reached. At that time, the cracks crossing this reinforcement widen noticeably. Shortly before failure, compression spalling and crushing the top face of the beam occurred adjacent to the loading plate. A side face of the half beam model is used to demonstrate

cracking sign. As shown in Fig. 10, at the nib of the beam at bottom, cracking signs refer to development normal tensile stresses in the $x$ (longitudinal) direction, and shear stresses in the $xz$ plane. Consequently, the direction of tensile principal stresses becomes inclined from the horizontal.
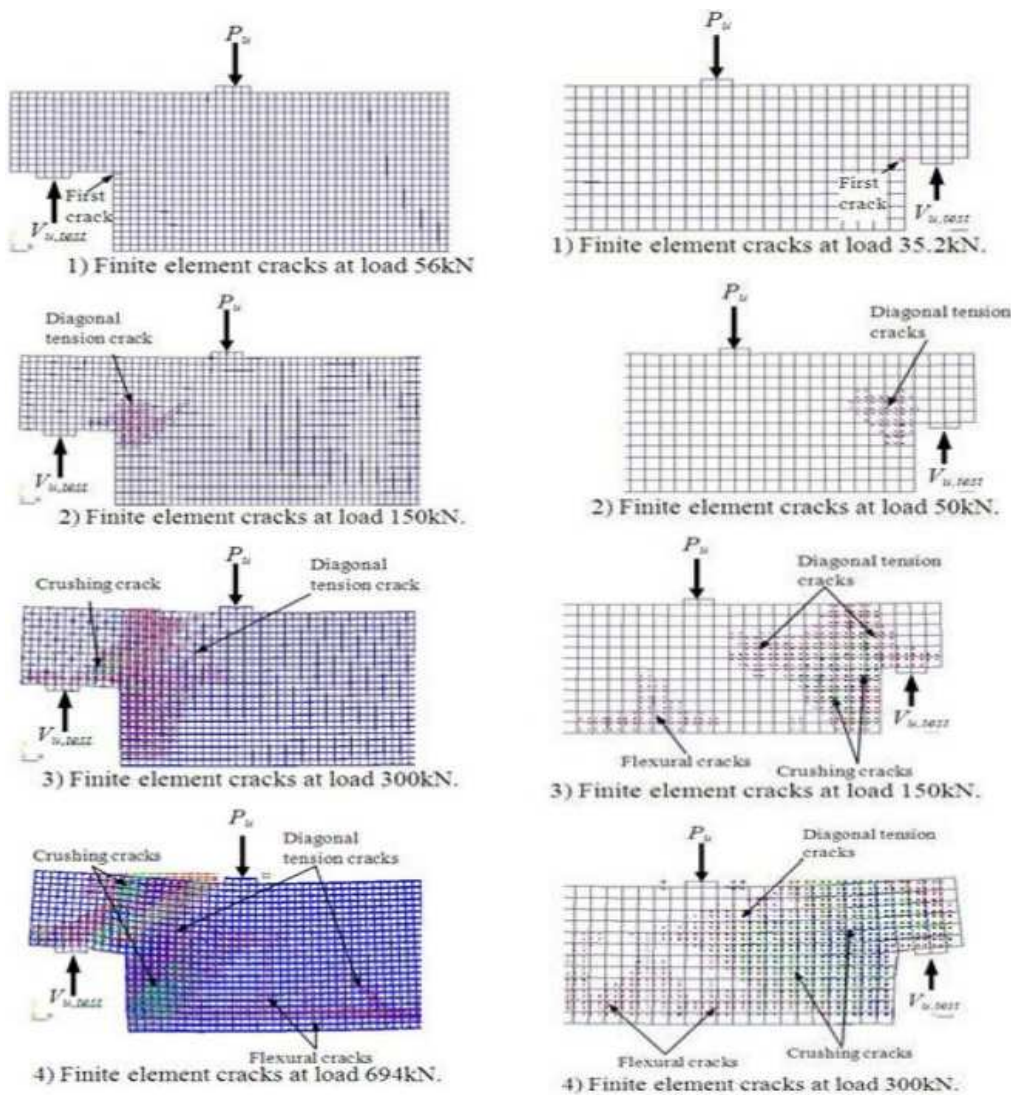
Fig. 10. Finite Element cracks at different loadvalues:
*a* – For specimen B56, *b* – For specimen B59

Once the principal tensile stresses exceed the ultimate tensile strength of the concrete, tensile cracks perpendicular to the directions of the principal stresses appear at integration points of the concrete finite elements. These are referred as diagonal tensile cracks.

Principal tensile stresses occur mostly in the longitudinal direction. When the principal stresses exceed the ultimate tensile strength of the concrete, cracking signs appear perpendicular to the principal stresses in that direction. Therefore, the cracking signs shown in Fig. 10 appear as vertical straight lines occurring at the integration points of the concrete solid elements. These are referred as flexural cracks. For a concrete structure subjected to uni-axial compression, cracks propagate primarily parallel to the direction of the applied compressive load since the cracks resulting from the tensile strains developed due to Poisson's ratio effect [12, 16]. Similar behavior is seen in Fig. 10 based on the finite element analysis. Loads in the z direction result in tensile strains in the y direction by Poisson's effect. Thus, circles appear perpendicular to the principal tensile strains in the y direction at the integration points in the concrete elements near the loading location referring to as compressive fracture.

**5. Parametric Study.** Using the developed the FE model that has been verified against the previous test results for reinforced concrete dapped end beam, a parametric study is conducted to beam B56 only, to evaluate the effects of shear span to depth ratio, compressive strength of concrete, and parameter of the main dapped end reinforcement. The details are described in Table 5.

Table 5. – Results summary of the parametric study

| Parameter | Value | Ultimate load FEM (kN) |
|---|---|---|
| Shear span / depth (a/d) | 0.78 | 650 |
| | 0.93 | 675 |
| | 1.12 | 725 |
| Concrete strength ($f'_c$) (MPa) | 25 | 660 |
| | 30 | 632 |
| | 40 | 600 |
| Parameter main dapped-end reinforcement ($\rho f_y$) (MPa) | 7.39 | 694 |
| | 3 | 275 |
| | 5 | 570 |

**5.1. Effect of Nominal Shear Span to Depth Ratio.** Fig. 11 Shows effect of the nominal shear span to depth ratio $a/d$ on the shear strength $V_d$ for dapped-end beam. It is seen that the shear strength of the beam increases with decreasing the nominal shear span to depth ratio $a/d$. The shear strength $V_d$, of beam B56 decreased from 482 kN for $a/d = 0.56$, to 383 kN for $a/d = 1.12$. This decrease in the shear strength is due to the cracks across depth of the nib of the beam, because when the shear span increases the flexural behavior becomes the controller instead of the shear failure, and cracks in the re-entrant corner of the beam develope. When the load further increases more cracks spread along depth of the nib and full depth of the beam, so that the beam should collapse at load level less than the beam with short shear span. Fig. 12 Shows the load-deflection relationship for B56 with different values of $a/d$ . Also it can be seen that the shear strength decreases with increasing the nominal shear span to depth ratio $a/d$ .
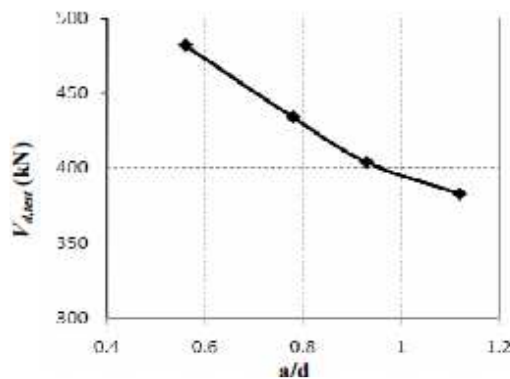


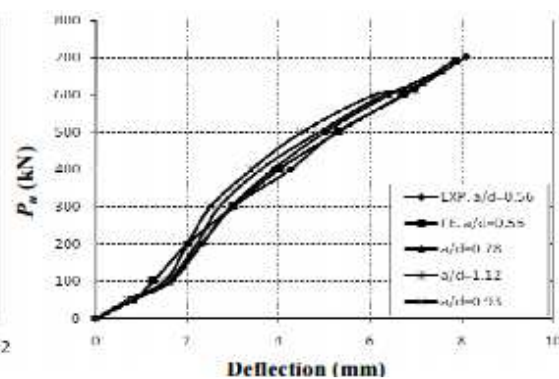Fig. 11. – Effect of a/d ratio on the shear strength of beam B56

Fig. 12. – Load-deflection curves for beam B56 for different values of a/d ratio

**5.2. Effect of Compressive Strength.** A parametric study is conducted using the present FE model with various concrete compressive cylinder strength values of 25, 30, and 40 MPa. The other parameters are the same for beam B56. The effect of compressive strength on the shear strength of beam B56 is illustrated in Fig. 13. The shear strength of dapped-end beams increases with the increase of the concrete compressive strength. Shear strength $V_d$, of the beam increases from 452 kN for $f'_c = 25$ MPa, to 504 kN for $f'_c = 40$ MPa. The amount of increase in shear strength is almost linearly proportional to compressive strength. The load-deflection behavior is illustrated in Fig. 14 for different values of concrete compressive strength. For all cases the initial values of deflection for the FE models are the same. Then when the load increases further differences is begin to be noticeable but less than the experimental values, expect for the case of $f'_c = 40$ MPa. In general load–deflection curves of the finite element models are almost upper then the experimental curve.
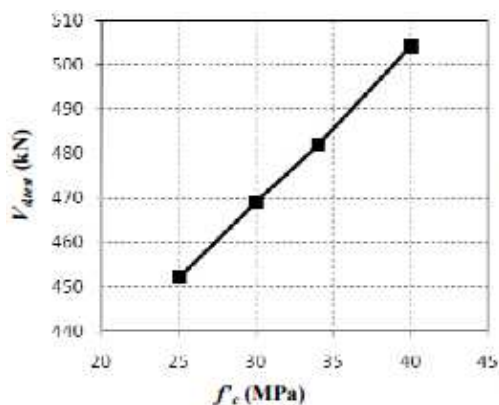


Fig. 13. – Effect of Concrete compressive strength on the shear strength of beam B56
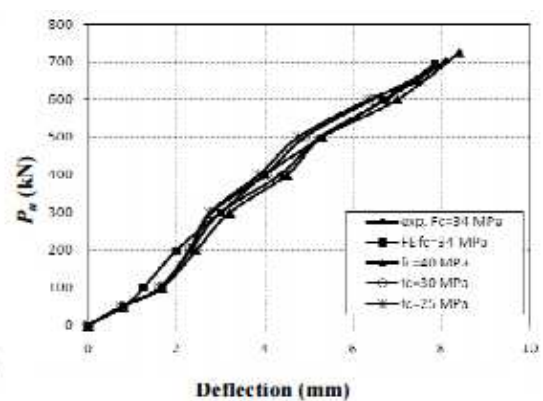
Fig. 14. – Load-deflection curves for beam B56 for different values of concrete compressive strength

**5.3. Effect of Main Dapped-End Reinforcement.** The parameter of main dapped-end reinforcement $\rho f_y$ is one of the most significant factors effecting the shear strength of reinforced concrete dapped-end beams. The FE models with various ρfy values of 3, 5, and 7.39 MPa are illustrated in Fig. 15. Shear strength of the beam increases with the increase of the main dapped-end reinforcement. Higher shear strength values are predicted for larger $\rho f_y$ values. The shear strength $V_d$ of the beam increase from 313 kN for $\rho f_y = 3$ MPa, to 482 kN for $\rho f_y = 7.39$ MPa. The load-deflection relationship is shown in Fig. 16 for different values of ρf$_y$, from which it is noticed that the shear strength values for the FE models are less than the experimental values.

On the other hand the deflection values in the earlier load applications are the same but when load increases further the difference begins to increase, especially for $\rho f_y = 3$ MPa, due to the small amount of area of reinforcement in the beam. In general and for all cases the main dapped-end reinforcement yielded before reaching the maximum applied load. Thus the load–deflection curve for FE models is slightly different from the experimental curve.
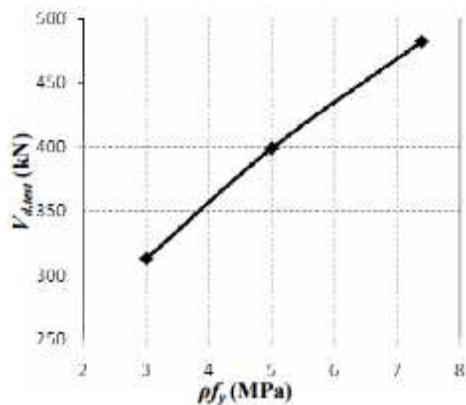


Fig. 15. – Effect of main dapped-end reinforcement
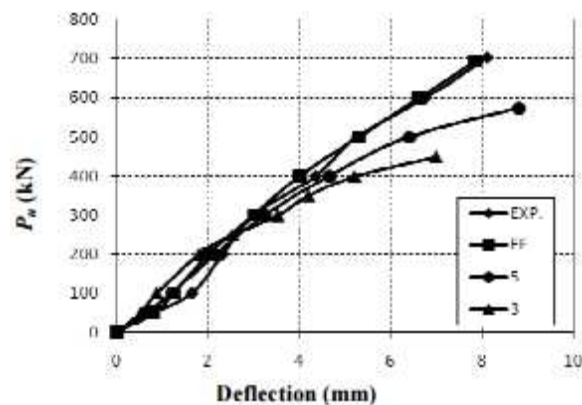on the shear strength of beam B56

Fig. 16. – Load-deflection curves for beam B56
for different amount of main reinforcement

**Conclusions.** A Finite element model has been developed to simulate the load–displacement behavior of the reinforced concrete dapped-end beams under static monotonic loading. The model takes into account the linear and nonlinear material properties for concrete and steel reinforcement. The FE model compared well with the results of previous experimental studies.

Parametric studies using this model has been carried out to investigate the effects of shear span to depth ratio, concrete compressive strength, and the amount the main dapped-end reinforcement on the behavior of the reinforced concrete dapped-end beams. From that comparison, and the parametric studies, the Following conclusions are drawn.

  – The predicted loads of the reinforced concrete dapped-end beams by the present FE models at various stages were found to be in good agreement with the previous test data.
  – The failure mechanism of reinforced concrete dapped-end beams is modeled quite well using the present FE model, and the failure load predicted is very close to the failure load of previous experimental studies.
  – Shear strength of the dapped-end beams increases with decreasing the nominal shear span to depth ratio (a/d). The shear strength Vd, of beam B56 is 482 kN for a/d = 0.56, and decreases to be 383 kN for a/d = 1.12.
  – Shear strength of the dapped-end beams linearly increases with the increase of the concrete strength for the studied beams.
  – Shear strength of the dapped-end beams linearly increases with the increase of the main dapped-end Reinforcement for the studied beams.

REFERENCES

1.    Mattock, A. H. Design and Behavior of Dapped-End Beams / A. H. Mattock, T. C. Chan // Journal of Structural Engineering, PCI Journal. 1979. – V. 24, No. 6. – P. 28–45.
2.    Shear Strength of High-Strength Concrete Dapped-End Beams / W. Y. Lu [et al.] // Journal of the Chinese Institute of Engineers. – 2003. – V. 26, No. 5. – P. 671–680.
3.    Crack Width Prediction Using Compatibility-Aided Strut-and-Tie Model / R. H. Ronnie // ACI Structural Journal. – 2003. – V. 100, No. – P. 413–421.

4. Foster, S. J. The Design of Nonflexural Members with Normal and High-Strength Concretes / S. J. Foster, R. I. Gilbert // ACI Structural Journal. – 1996. – V. 93, No. 1. – P. 3–10.

5. Building Code Requirements for Structural Concrete (ACI 318-2008) and Commentary (318R-2008) / American Concrete Institute. – Farmington Hills, Mich., 2008.

6. Marti, P. Basic Tools of Reinforced Concrete Beam Design / P. Marti // ACI JOURNAL, Proceedings. – 1985. – V. 82, No. 1. – P. 46–56.

7. Mirza, S. A. Strength Criteria for Concrete Inverted T-Girders / S. A. Mirza, R. W. Furlong // Journal of Structural Engineering, ASCE. – 1983. – V. 109, No. 8. – P. 1836–1853.

8. Mirza, S. A. Design of Reinforced and Prestressed Concrete Inverted T-Beams for Bridge Structures / S. A. Mirza, R. W. Furlong // PCI Journal. – 1985. – V. 30, No. 4. – P. 112–136.

9. Siao, W. B. Shear Strength of Short Reinforced Concrete Walls, Corbels, and Deep Beams / W. B. Siao // ACI Structural Journal – 1994. – V. 91, No. 2. – P. 123–132.

10. Swanson Analysis System / ANSYS. – US, 2003.

11. Schlaich, J. Towards a Consistent Design of Structural Concrete / J. Schlaich, K. Schafer, M. Jennewein // PCI Journal. – 1987. – V. 32, No. 3. – P. 74–150.

12. Willam, K.J. Constitutive model for triaxialbehaviour of concrete. In: Seminar on concrete structures subjected to triaxial stresses / K.J. Willam, E.P. Warnke // International association of bridge and structural engineering conference. – Bergamo, 1974. – P. 174.

13. Wolanski, A. J. Flexural Behavior of Reinforced and Prestressed Concrete Beams Using Finite Element Analysis / A. J. Wolanski // Master thesis, Marquette University. – Milwaukee, Wisconsin, 2004.

14. MacGregor, J.G. (1992) "Reinforced concrete mechanics and design / J.G. MacGregor // Englewood Cliffs. – NJ : Prentice-Hall, Inc., 1992.

15. Job, T. Finite Element Analysis of Shear Critical Prestressed SFRC Beams / T. Job, R. Anath // Computers and Concrete. – 2006. – Vol. 3, No. 1. – P. 65–77.

16. Shah, S.P. Fracture mechanics of concrete / S.P. Shah, S.E. Swartz, C. Ouyang. – NY : John Wiley & Sons, Inc., 1995.